On wake vortex response for all combinations of five classes of aircraft

L. M. B. C. Campos and J. M. G. Marques
Secção de Mecânica Aeroespacial, Instituto Superior Técnico
Lisbon, Portugal

ABSTRACT

The present paper concerns the response of a following airplane to a pair of wing tip vortices left by a leading aircraft, represented by the Hallock-Burnham model, including the effect of vorticity decay between the two aircraft. The effect of vorticity is evaluated in terms of the induced rolling moment and also the lift loss; these specify the roll acceleration and the downward acceleration, respectively. The corresponding two response equations can be put into the same dimensionless form, and integrated using exponential integrals. This specifies the roll rate and sink rate as a function of time; besides the latter, the bank angle and altitude loss, are also plotted, all also as a function of time, for all combinations of leading and following aircraft in five classes. These are the three ICAO weight categories of light, medium and heavy, plus two other cases, *viz* the special case of the Boeing 757, which requires larger separations distances, and the case of a future very large transport aircraft (VLTA) exceeding significantly the size of a Boeing 747.

NOMENCLATURE

a	core radius for identical vortices $a_r = a_t \equiv a$, Equation (1)
a_r, a_t	core radius of the right, left wing tip vortices, Equation (5)
b	wing span, Equation (6)
c	wing chord, Equation (6)
$\overline{c}$	geometric mean wing chord, Equation (8b)
c_r	root chord, Equation (9a)
c_t	tip chord, Equation (9b)
$\vec{e}_x, \vec{e}_y, \vec{e}_z$	base vectors, Equation (34a,b)
f_r, f_t	average encounter factor for lift loss, Equation (49)
$f_{1r}, f_{2r}, f_{3r}, f_{4r}$,	left, right encounter factor for lift loss, Equation (27)
g	terms in encounter factors, Equation (28a-d)
h	Earth's gravitational acceleration, Equation (51)
	average encounter factor for rolling moment, Equation (54)
h_r, h_ℓ	left, right encounter factor for rolling moment, Equation (30)
ℓ	lift per unit span, Equation (11)
$\Delta\ell$	lift loss per unit span due to wake, Equation (14)
m	aircraft mass, Equation (46)
r	radial distance from vortex axis, Equation (1)
r_2	radius of gyration, Equation (57)
t	time, Equation (31)
t_0	time scale, Equation (88a)
t_*	time of peak vorticity, Equations (77)(85a)
$\tilde{t}$	dimensionless time, Equation (88a)
$\tilde{t}_1$	dimensionless time delay, Equation (91a)
w	downwash velocity, Equation (1)
x	longitudinal co-ordinate, Equation (34a)
y	lateral co-ordinate, Equation (5)
y_r, y_ℓ	lateral distance of right, left vortex from aircraft axis, Equation (5)
y_0	lateral offset of following relative to leading aircraft, Fig. 2
z	altitude, Equation (34a)
$\dot{z}$	sink speed, Equation (76a)
$\ddot{z}$	downward acceleration, Equation (46)
A	dimensionless aircraft response parameter, Equation (61, 64)
B	aircraft response parameter, Equation (76b)
C_L	wing lift coefficient, Equation (42)
$\bar{C}_L$	sectional lift coefficient, Equation (11)
$C_{L\alpha}$	sectional lift slope, Equation (12a)
C_1, C_2	constants in vorticity decay function, Equation (90)
D	aircraft response parameter, Equation (78b)
$E(...)$	exponential integral, Equation (67)
I	rolling moment of inertia, Equation (52)
I_{1r}, I_{2r}	integrals, Equation (22a,b)
I_{3r}, I_{4r}	integrals, Equation (24a,b)
ΔL	total lift loss, Equation (15)

Paper No. 2718. Manuscript received 31 August 2001, revised version received 23 October 2003, accepted 8 April 2004.

https://doi.org/10.1017/S0001924000000154 Published online by Cambridge University Press

R	rolling moment induced by wake, Equation (16)
S	wing area, Equation (29)
T	inverse dimensionless time, Equation (66)
T_1, T_2	inverse dimensionless time at start and end of wake encounter, Equation (70)
U	incident flow velocity, Equation (11)
$\vec{v}$	total flow velocity, Equation (31)
W	aircraft weight, Equation (43)
X	dimensionless response variable, Equation (61a, 64a)
α	angle-of-attack of incident stream, Equation (12a)
α_e	difference between angle-of-attack α and self-wake downwash angle
α_{dw}	self-wake downwash angle, Equation (12a)
$\bar{\alpha}$	angle-of-attack due to downwash, Equation (12b)
$\delta(...)$	Dirac delta function, Equation (37)
λ	taper ratio of wing planform, Equation (8a)
ϕ	roll angle, Equation (64a)
$\dot{\phi}$	roll rate, Equation (78a)
$\ddot{\phi}$	roll acceleration, Equation (52)
η	shear viscosity, Equation (31)
ζ	bulk viscosity, Equation (31)
ξ	integration variable, Equation (67)
ω	dimensionless vorticity with time delay, Equation (87)
$\bar{\omega}$	dimensionless vorticity, Equation (86)
ρ	mass density of air, Equation (11)
τ	dimensionless time, Equation (59a)
τ_1, τ_2	dimensionless time at start and end of encounter, Equation (68)
υ	dimensionless viscosity, Equation (88b)
Ω	vorticity, Equation (2)
Ω_r, Ω_ℓ	vorticity of right, left vortex, Equation (5)
Ω_{max}	peak vorticity, Equation (85b)
Γ	circulation, Equation (41)
Γ_0	wing vortex strength, Equation (1)

Subscripts

1	leading aircraft, e.g. chord c_1
2	following aircraft, e.g. chord c_2
h	heavy aircraft ($W > 136t$)
ℓ	light aircraft ($W < 7t$)
m	medium aircraft ($7t < W < 136t$)
s	special aircraft
v	very large aircraft

Abbreviations

ICAO	International Civil Aviation Organization
FAA	Federal Aviation Administration
HB	Hallock-Burnham
SSD	safe separation distance
VLTA	very large transport aircraft

1.0 INTRODUCTION

The effects of the wake of a leading aircraft on a following aircraft are one of the main factors determining separation distances on landing and take-off. Thus wake effects have implications both on:

(*i*) airplane safety in terms of it ability to retain roll control and contain height loss;
(*ii*) runway capacity determined by aircraft spacing, which then impacts airport capacity and air traffic capacity. In addition, wake effects relate to aircraft design, in the sense that it is desirable to;
(*iii*) reduce the strength of the wake of the leading aircraft;
(*iv*) reduce the susceptibility of the following aircraft to wake effects.

Thus the subject of wake effects relates both to aircraft design and air traffic management, justifying the existence of vast literature on the subject (more than 1,800 references to 'wake', 'vortex' and 'wake vortex' on NASA and similar data bases).

The specification of wake effects can lead to:

(a) either the determination of a safe separation distance (SSD), beyond which the following aircraft has enough roll control authority to cope with the wake of the leading aircraft;
(b) the calculation of the response of the following aircraft to the wake of the leading aircraft at any distance.

The knowledge of aerodynamics and flight dynamics required[1] is comparable in the two cases, the main difference being that the vorticity should be expressed as a function of distance to calculate the SSD in case (a), and as a function of time to calculate response in case (b). The response to wake effects may include, in addition to the roll effect, also an altitude loss; the two effects can combine to present a safety hazard, e.g. if a wake is encountered close to the ground in a landing approach.

Most of the vast literature on wake effects, of which a few examples are given[2-6], estimates wake effects using numerical methods. Analytical models have been developed assuming constant vortex strength[7]. The present model takes into account vortex decay in the analytical calculation of airplane response to a wake, as follows:

(*i*) the lift loss (see Section 2) and rolling moment (see Section 3) due two wing tip vortices with axis parallel to the following aircraft are calculated;
(*ii*) both involve the vorticity, whose decay with time is specified (see Section 4) by dissipation by viscosity and convection in the downwash of the leading aircraft;
(*iii*) this specifies the rolling moment and lift loss of the following aircraft as a function of time, and thus the response (see Section 5) in terms of roll and downward acceleration, respectively;
(*iv*) the integration in dimensionless form leads to an exponential integral in both cases, which is found in Table 8 and specifies (see Section 6) the roll rate and sink speed;
(*v*) besides these, the bank angle and altitude loss, are also plotted as a function of time, for all (see Section 7) combinations of leading and following aircraft in five categories: light, medium, special, heavy and very large;
(*vi*) the reduction in wake effects as the vortex is encountered later is its lifetime is considered (see Section 8) . The discussion (see Section 9) includes a comparison of the vorticity decay model with flight test measurements from the Memphis data base.

2.0 EFFECT OF WAKE ON LIFT LOSS

There are several vortex models, e.g. those of Rankine[9], Lamb-Oseen[10], Hoffman-Joubert[11], Hallock-Burnham[12] and Proctor[13]. The difference between different vortex models is probably no greater than other uncertainties in the calculation of aircraft response to wake vortices. Thus the choice of a vortex model may not be critical, and the Hallock-Burnham model is chosen here because it has three desirable features:

(*i*) it fits well with experimental data;
(*ii*) it is specified by a single analytical expression valid for all radial distances from the 'core' to the 'external flow';
(*iii*) the analytical expression is of simple algebraic form, amenable to straightforward integration, to calculate induced lift loss and rolling moment.

https://doi.org/10.1017/S0001924000000154 Published online by Cambridge University Press

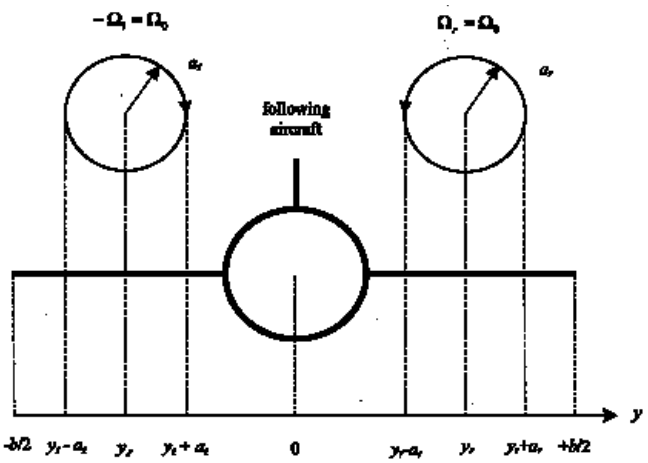


Figure 1. Interaction of following aircraft with two wing tip vortices of leading aircraft, with paralel axis and asymmetric positions and different radii and vorticities.

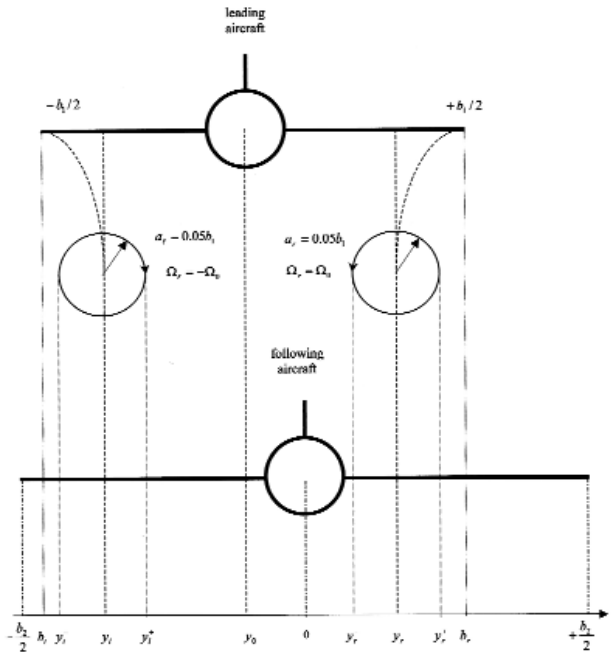


Figure 2. Leading aircraft with elliptic loading trailing two wing tip vortices, encountered by the following aircraft, flying along a parallel path, offset by a lateral distance y_0 from the axis.

The tangential velocity of the Hallock-Burnham (HB) vortex is given as a function of radial distance r as by:

$$w(r)=\frac{\Gamma_0}{2\pi}\frac{r}{r^2+a^2} \quad \ldots (1)$$

The tangential velocity is zero at the centre, $w(0) = 0$ grows linearly for small distance compared with the vortex core radius $w(r)\sim\Gamma_0\, r/(2\pi a^2)$ for $r^2 << a^2$, and matches smoothly to a potential flow decay at large distances $w(r)\sim\Gamma_0\, r/(2\pi r)$ for $r^2 >> a^2$, going through a maximum at the vortex core radius:

$$w_{\max} \equiv w(a)=\Gamma_0/4\pi a=\Omega a/4 \quad \ldots (2)$$

this value being used to specify the reference vorticity , and to relate it to wake vortex strength:

$$\Gamma_0=\pi a^2\Omega \quad \ldots (3)$$

The vorticity will be reconsidered in Section 4. Thus the HB-vortex model is specified by:

$$2w(r)=\frac{\Omega a^2 r}{r^2+a^2} \quad \ldots (4)$$

for a single vortex with axis at the origin. In the case (Fig. 1) of a following aircraft encountering two wing tip vortices, parallel to its axis, at positions y of the right and y_ℓ for the left vortex, with vorticities respectively Ω_r and $-\Omega_\ell$, the downwash velocity is:

$$2w(y)=\Omega_r a_r^2\frac{y-y_r}{a_r^2+(y-y_r)^2}-\Omega_\ell a_\ell^2\frac{y-y_\ell}{a_\ell^2+(y-y_\ell)^2} \quad \ldots (5)$$

The way in which the configuration in Fig. 1 may arise, is further explained in Fig. 2:

(*i*) the leading aircraft leaves two wing tip vortices, in the symmetric case with opposite vorticities $\Omega_r = \Omega_0 = -\Omega_l$ and core radii $a_r = a_\ell = 0{\cdot}05b_1$ where b_1 is the span;
(*ii*) the following aircraft has span b and flies parallel to the vortex axis, at a lateral distance y_0 from the centreline.

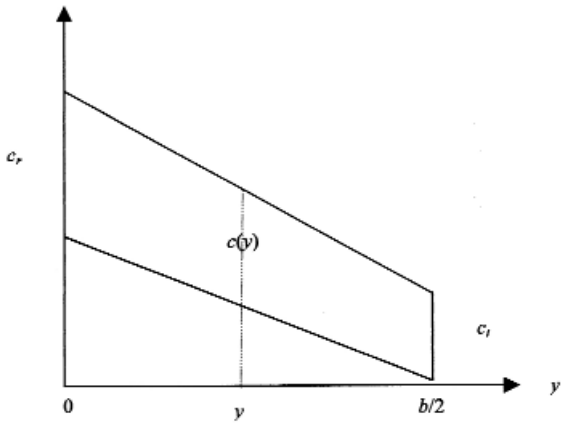


Figure 3. Trapezoidal wing planform showing chord at arbitrary station, and at root and tip.

The location y_t , y_ℓ of the vortices and the vortex core radii a_r , a_ℓ , relative to the wing span, and the magnitude of the vorticities Ω_r , Ω_l are unrestricted, *viz* Figs 1 and 2 represent vortices entirely within the aircraft span, but either vortex could be outside span or only partly inside.

Next is considered a trapezoidal wing (Fig. 3), i.e. with straight leading and trailing edges and chord c_r at the root and c_t at the tip, so that the chord at a arbitrary position is given by:

$$c(y)=c_r+(c_t-c_r)\frac{2|y|}{b} \quad \ldots (6)$$

https://doi.org/10.1017/S0001924000000154 Published online by Cambridge University Press

The root, Equation (7a) and tip Equation (7b) chords:

$$c(0)=c_r\ ,\quad c(\pm b/2)=c_t \qquad \ldots (7a,b)$$

specify the taper ratio Equation (8a) and geometric mean chord Equation (8b):

$$\lambda\equiv\frac{c_t}{c_r},\quad \bar{c}=\frac{(c_t+c_r)}{2} \qquad \ldots (8a,b)$$

or inversely:

$$c_r=\frac{2\bar{c}}{1+\lambda},\quad c_t=\frac{2\lambda\bar{c}}{1+\lambda} \qquad \ldots (9a,b)$$

Substitution of Equation (9a,b) in Equation (6) specifies

$$c(y)=\frac{2\bar{c}}{1+\lambda}\left[1+(\lambda-1)\frac{2|y|}{b}\right] \qquad \ldots (10)$$

the chord at an arbitrary station, as a function of mean chord and taper ratio.

The lift per unit span[14] is given by:

$$l(y)=\frac{1}{2}\rho\bar{C}_L(\alpha)U^2c(y) \qquad \ldots (11)$$

and below the stall the sectional lift coefficient is a linear function of angle of attack:

$$\bar{C}_L(\alpha)=C_{L_\alpha}(\alpha_e-\bar{\alpha})=C_{L_\alpha}(\alpha-\alpha_{dw}-\bar{\alpha}) \qquad \ldots (12a)$$

where $\alpha_e=\alpha_{dw}-\alpha_{dw}$ is the difference between the angle-of-attack and the self-wake downwash angle; in lifting line theory the latter may vary along the span $\alpha_{dw}(y)$, together with the sectional lift $l(y)$ and downwash velocity $w(y)$. The lift slope $C_{L\alpha}$ is 2π for the Joukowsky airfoil[15] and takes values of that order of magnitude for other airfoils[16]. The lift is taken to be zero when aligned with the incident stream:

$$\bar{\alpha}=\frac{w(y)}{U} \qquad \ldots (12b)$$

The substitution of Equation (12b) into (12a) specifies Equation (11):

$$l(y)=\frac{1}{2}C_{L_\alpha}\rho c(y)U[U\alpha-w(y)] \qquad \ldots (13)$$

the lift per unit span which is correct to first order in the downwash velocity $w(y)$. The lift loss per unit span due to the wake of leading aircraft impinging on the following aircraft is given by the second term on the right hand side of Equation (13):

$$\Delta l(y)=-\frac{1}{2}C_{L_\alpha}\rho Uc(y)w(y) \qquad \ldots (14)$$

and thus

$$\Delta L=-\frac{1}{2}C_{L_\alpha}\rho U\int_{-b/2}^{b/2}c(y)\ w(y)\ \mathrm{d}y \qquad \ldots (15)$$

specifies the total lift loss due to the vortex encounter. In this formula the lift coefficient was assumed to be a linear function of angle-of-attack Equation (12a); in the applications that follow, the vortex encounter causes a lift loss, and thus a reduction of angle-of-attack. Thus, the airplane moves away from stall; the assumption of linear lift coefficient should hold for the initial disturbed motion.

3.0 ROLLING MOMENT INDUCED BY WAKE

Another effect of the vortex encounter is the rolling moment induced on the following aircraft by the wake of the leading aircraft:

$$R=\int_{-b/2}^{b/2}y\ \Delta l(y)\ \mathrm{d}y \qquad \ldots (16)$$

which relates to the lift loss Equation (14) per unit span:

$$R=-\frac{1}{2}C_{L_\alpha}\rho U\int_{-b/2}^{b/2}y\ w(y)\ c(y)\ \mathrm{d}y \qquad \ldots (17)$$

Using the chord Equation (10) for a trapezoidal wing and downwash Equation (5) for two dissimilar HB-vortices, the integrals:

$$2\Delta L=-\frac{C_{L_\alpha}\rho U\bar{c}\Omega_r a_r^2}{1+\lambda}\int_{-b/2}^{b/2}\left(1+\frac{\lambda\text{-}1}{\mathrm{b}}2|y|\right)\frac{y-y_r}{a_r^2+(y-y_r)^2}\ \mathrm{d}y$$
$$+\frac{C_{L_\alpha}\rho U\bar{c}\Omega_l a_l^2}{1+\lambda}\int_{-b/2}^{b/2}\left(1+\frac{\lambda\text{-}1}{\mathrm{b}}2|y|\right)\frac{y-y_l}{a_l^2+(y-y_l)^2}\ \mathrm{d}y, \qquad \ldots (18)$$

$$2R=-\frac{C_{L_\alpha}\rho U\bar{c}\Omega_r a_r^2}{1+\lambda}\int_{-b/2}^{b/2}\left(1+\frac{\lambda\text{-}1}{\mathrm{b}}2|y|\right)\frac{y-y_r}{a_r^2+(y-y_r)^2}y\mathrm{d}y+$$
$$+\frac{C_{L_\alpha}\rho U\bar{c}\Omega_l a_l^2}{1+\lambda}\int_{-b/2}^{b/2}\left(1+\frac{\lambda\text{-}1}{\mathrm{b}}2|y|\right)\frac{y-y_l}{a_l^2+(y-y_l)^2}y\mathrm{d}y, \qquad \ldots (19)$$

specify the lift loss Equation (18) and the rolling moment Equation (19). The integrals will be evaluated the change of variable:

$$u=(y-y_r)/a_r \qquad \ldots (20)$$

for the right-hand vortex, and similarly for the left-hand vortex.

The lift loss Equation (18):

$$2\Delta L=-\frac{C_{L_\alpha}\rho U\bar{c}\Omega_r a_r^2}{1+\lambda}\left(I_{1r}+2\frac{\lambda-1}{b}I_{2r}\right)$$
$$+\frac{C_{L_\alpha}\rho U\bar{c}\Omega_l a_l^2}{1+\lambda}\left(I_{1l}+2\frac{\lambda-1}{b}I_{2l}\right) \qquad \ldots (21)$$

involves the integrals for rectangular wings:

$$I_{1r}\equiv\int_{-b/2}^{b/2}\frac{y-y_r}{a_r^2+(y-y_r)^2}\mathrm{d}y=\int_{-(b/2+y_r)/a_r}^{(b/2-y_r)/a_r}\frac{u}{1+u^2}\mathrm{d}u \qquad \ldots (22a)$$

and the trapezoidal wing correction:

$$I_{2r}\equiv\int_{0,0}^{b/2,-b/2}\frac{y(y-y_r)}{a_r^2+(y-y_r)^2}\mathrm{d}y=$$
$$\int_{-y_r/a_r,-y_r/a_r}^{(b/2-y_r)/a_r,-(b/2+y_r)/a_r}\frac{u(y_r+a_ru)}{1+u^2}du \qquad \ldots (22b)$$

where the second integral is taken twice at each limit. The rolling moment Equation (18):

$$2R=-\frac{1}{1+\lambda}C_{L_\alpha}\rho U\bar{c}b\left[\Omega_r a_r^2\left(I_{3r}+2\frac{\lambda-1}{b}I_{4r}\right)\right.$$
$$\left.-\Omega_l a_l^2\left(I_{3l}+2\frac{\lambda-1}{b}I_{4l}\right)\right] \qquad \ldots (23)$$

involves the integrals for the rectangular wings:

https://doi.org/10.1017/S0001924000000154 Published online by Cambridge University Press

$$bI_{3r} \equiv \int_{-b/2}^{b/2} \frac{y\left(y-y_r\right)}{a_r^2+\left(y-y_r\right)^2}\mathrm{d}y = \int_{-(b/2+y_r)/a_r}^{(b/2-y_r)/a_r} \frac{u\left(y_r+a_r u\right)}{1+u^2}\mathrm{d}u \quad \ldots (24a)$$

and the trapezoidal wing correction:

$$bI_{4r} \equiv \int_{0,0}^{b/2,-b/2} \frac{y^2\left(y-y_r\right)}{a_r^2+\left(y-y_r\right)^2}\mathrm{d}y = \int_{-y_r/a_r,-y_r/a_r}^{(b/2-y_r)/a_r,-(b/2+y_r)/a_r} \frac{y_r^2 u+2y_r a_r u^2+a_r^2 u^3}{1+u^2}\mathrm{d}u \quad \ldots (24b)$$

The four integrals Equations (22a,b) and (24a,b) involve only three primitives:

$$\int \frac{u}{1+u^2}\mathrm{d}u = \frac{1}{2}\log\left(1+u^2\right) \quad \ldots (25a)$$

$$\int \frac{u^2}{1+u^2}\mathrm{d}u \equiv \int\left(1-\frac{1}{1+u^2}\right)\mathrm{d}u = u-\mathrm{Arctan}\,u \quad \ldots (25b)$$

$$\int \frac{u^3}{1+u^2}\mathrm{d}u = \int\left(u-\frac{u}{1+u^2}\right)\mathrm{d}u = \frac{u^2}{2}-\frac{1}{2}\log\left(1+u^2\right) \quad \ldots (25c)$$

using these the lift loss Equation (11) and the rolling moment Equation (23) are evaluated for dissimilar vortices and zero bank angle. The reverse case of similar vortices and non-zero bank angle has been treated elsewhere[17].

Substitution of Equation (25a,b) in Equation (22a,b), specifies the lift loss Equation (21) as:

$$\Delta L = -\frac{1}{1+\lambda}C_{L_\alpha}\rho U\bar{c}\left(\Omega_r a_r^2 f_r - \Omega_\ell a_\ell^2 f_\ell\right) \quad \ldots (26)$$

where the dimensionless factor:

$$4f_r = f_{1r} + \frac{\lambda-1}{b}\left(2y_r f_{2r} + 4a_r f_{3r}\right) \quad \ldots (27)$$

involves Equation (28a,b,c), and thus depends on the encounter geometry:

$$f_{1r} \equiv \log\left[\frac{\left(b/2-y_r\right)^2+a_r^2}{\left(b/2+y_r\right)^2+a_r^2}\right] \quad \ldots (28a)$$

$$f_{2r} \equiv \log\left[\frac{\left(a_r^2+b^2/4+y_r^2\right)^2-b^2y_r^2}{\left(a_r^2+y_r^2\right)^2}\right] \quad \ldots (28b)$$

$$f_{3r} \equiv \mathrm{Arctan}\left[\left(b/2+y_r\right)/a_r\right] - \mathrm{Arctan}\left[\left(b/2-y_r\right.\right. \\ -2\mathrm{Arctan}\left(y_r/a_r\right) \quad \ldots (28c)$$

$$f_{4r} \equiv \mathrm{Arctan}\left[\left(b/2+y_r\right)/a_r\right] + \mathrm{Arctan}\left[\left(b/2-y_r\right)/a_r\right] \quad \ldots (28d)$$

The same factors Equation (28a-d) appear in the rolling moment Equation (23), when Equation (25a,b,c) are substituted in Equation (24a,b), *viz*:

$$R = -\frac{1}{1+\lambda}C_{L_\alpha}\rho US\left(\Omega_r a_r^2 h_r - \Omega_r a_l^2 h_l\right) \quad \ldots (29)$$

where:

$$4h_r = 2+\left(y_r/b\right)f_{1r} - 2\left(a_r/b\right)f_{4r} + \left(\lambda-1\right) \\ \left\{+2\left[\left(y_r^2-a_r^2\right)/b^2\right]f_{2r} + 8\left(a_r y_r/b^2\right)f_{3r}\right\} \quad \ldots (30)$$

These expressions simplify in the case of equal vorticities $\Omega_l = \Omega_r$, vortex core radii $a_l = a_r$ or symmetrical vortices $y_l = y_r$. In general Equations (27) and (30) reduce to the first terms for a rectangular wing $\lambda = 1$, and for a trapezoidal wing there is the correction specified by the factor multiplying $(\lambda - 1)$.

4.0 VORTICITY DECAY WITH TIME DUE TO VISCOSITY

The dependence of the rolling moment Equation (29) and lift loss Equation (26) on time is specified by the vorticities $\Omega_r(t)$ and $\Omega_l(t)$. Starting from the Navier-Stokes equation[18]

$$\frac{\partial\vec{V}}{\partial t} + \nabla\left(V^2/2\right) + \left(\nabla\times\vec{V}\right)\times\vec{V} + \rho^{-1}\nabla p = \eta\nabla^2\vec{V} \cdot \\ + \left(\varsigma+\eta/3\right)\nabla\left(\nabla.\vec{V}\right) \quad \ldots (31)$$

in the incompressible case $\nabla.\vec{V} = 0$ or $\rho = const$, by taking the curl, leads to a convected diffusion equation,

$$\nabla.\vec{V} = 0, \quad \frac{\partial\vec{\Omega}}{\partial t} + \nabla\times\left(\vec{\Omega}\times\vec{V}\right) = \eta\nabla^2\vec{\Omega} \quad \ldots (32)$$

satisfied by the vorticity:

$$\vec{\Omega} \equiv \nabla\times\vec{V} \quad \ldots (33)$$

In the present case of mean flow velocity consisting of an uniform stream plus a downwash Equation (34a)

$$\vec{V} = U\vec{e}_x + w\vec{e}_z, \quad \vec{\Omega} = \Omega\vec{e}_x \quad \ldots (34a,b)$$

and vorticity is aligned with the aircraft axis Equation (34b), and the second term of the vorticity equation Equation (32) is:

$$\nabla\times\left(\vec{V}\times\vec{\Omega}\right) = \vec{e}_x\frac{\partial(w\Omega)}{\partial z} - \vec{e}_z\frac{\partial(w\Omega)}{\partial x} \quad \ldots (35)$$

if longitudinal derivatives are smaller than transverse ones, the first term in Equation (35) predominates.

In the latter case the vorticity equation reduces to its *x*-component, *viz*.

$$\frac{\partial}{\partial x} << \frac{\partial}{\partial y}, \frac{\partial}{\partial z}: \quad \frac{\partial\Omega}{\partial t} + \frac{\partial\left(w\Omega\right)}{\partial z} = \eta\left(\frac{\partial^2\Omega}{\partial y^2} + \frac{\partial^2\Omega}{\partial z^2}\right) \quad \ldots (36)$$

This is a scalar heat equation[19], with convective term. A point vortex of circulation strength Γ_0 is taken as the source:

$$\frac{\partial\Omega}{\partial t} + \frac{\partial\left(w\Omega\right)}{\partial z} - \eta\left(\frac{\partial^2\Omega}{\partial y^2} + \frac{\partial^2\Omega}{\partial z^2}\right) = \Gamma_0\delta\left(x\right)\delta\left(y\right) \quad \ldots (37)$$

with δ denoting the Dirac delta function. The solution of Equation (37) is Ref. 20:

$$\Omega(t,y,z) = \frac{\Gamma_0}{2\pi\eta\left(t-z/w\right)}\exp\left(-\frac{y^2+z^2}{2\eta\left(t-z/w\right)}\right) \quad \ldots (38)$$

The wake of the leading aircraft is thus represented at the following aircraft as a point vortex of circulation strength Γ_0, which is an approximate representation if the two aircraft are at a large distance compared to wing parameters. The transverse coordinates disappear from the vorticity Equation (38) by identifying them with the vortex radius:

$$y^2+z^2 = a^2: \quad \Omega\left(t,z\right) = \frac{\Gamma_0}{2\pi\eta\left(t-z/w\right)}\exp\left(-\frac{a^2}{2\eta\left(t-z/w\right)}\right) \quad \ldots (39)$$

https://doi.org/10.1017/S0001924000000154 Published online by Cambridge University Press

The longitudinal coordinate may also be omitted if the separation between the aircraft is large enough:

$$t = x/U >> z/w: \quad \Omega(t) = \frac{\Gamma_0}{2\pi\eta t}\exp\left(-\frac{a^2}{2\eta t}\right) \qquad \ldots (40)$$

leaving only the time dependence in the vorticity.

The vorticity Equation (40) is proportional to the vortex circulation strength Γ_0 of the leading aircraft, which is calculated next. The lift per unit span is given by the Joukowski theorem[14,15].

$$l(y) = \rho U \Gamma(y) \qquad \ldots (41)$$

so that comparison with Equation (11) specifies the circulation

$$\Gamma(y) = \frac{1}{2} C_L(\alpha) U c(y) \qquad \ldots (42)$$

where $C_L(\alpha)$ is the lift wing coefficient. For straight steady and level flight the weight equals the lift:

$$W = \frac{1}{2}\rho U^2 S C_L(\alpha) \qquad \ldots (43)$$

and hence the vortex strength is specified by the circulation at the wing root:

$$\Gamma_0 \equiv \Gamma(0) = \frac{1}{2} C_L(\alpha) U c_r = \frac{c_r W}{\rho U S} \qquad \ldots (44)$$

in terms of aircraft parameters. The vorticity Equation (40) represents the rolled-up part of the vortex, and is zero at the trailing edge of the leading aircraft $\Omega(0) = 0$; it then increases with time as the vortex rolls up, reaching a maximum $\Omega_{max} = \Gamma_0/(2\pi a^2\rho)$ at a time $t_* = a^2/2\eta$, after which the viscosity, besides limiting growth, causes ultimate decay $\Omega(\infty) = 0$. Substitution of Equation (44) in Equation (40) specifies the vorticity laws:

$$\Omega(t) = \frac{c_{r_1} W_1}{2\pi\rho U_1 S_1 \eta t}\exp\left(-\frac{a^2}{2\eta t}\right) \qquad \ldots (45)$$

where the index '1' refers to the leading aircraft (it is omitted in , since the vortex core radius only appears for the leading aircraft).

5.0 AIRPLANE RESPONSE TO THE WAKE ENCOUNTER

The downward acceleration

$$m\ddot{z} = \Delta L \qquad \ldots (46)$$

is associated with the lift loss Equation (26). The vortex radii will be taken the same $a_l = a_r = a$, so that the vorticity decay law Equation (45) is the same for the right and the left hand vortices:

$$a_l = a_r = a: \quad 2\Omega_\pm(t) \equiv \Omega_r(t) \pm \Omega_l(t) \qquad \ldots (47a,b)$$

and it will be shown in the sequel that:

(*i*) the sum of vorticities is relevant to the lift loss;
(*ii*) the difference of vorticities is relevant to the rolling moment.

Using Equation (47), the lift loss Equation (26) is given by:

$$\Delta L = -\frac{2}{1+\lambda} C_{L_\alpha} \rho U \bar{c} a^2 \Omega_+(t) f \qquad \ldots (48)$$

where the average encounter factor f for the lift loss is defined by:

$$\Omega_r f_r - \Omega_l f_l \equiv f(\Omega_r + \Omega_l) = 2f\Omega_+ \qquad \ldots (49)$$

This will be obviously met by symmetrical vortices, since $y_r = -y_l$ implies $f_r = -f_l \equiv f$ by Equation (27) and Equation (28a-d) and then Equation (49) reduces to Equation (47a); for opposite right and left vorticites $\Omega_r = \Omega_l = \Omega_0$, it follows that $\Omega_+ = 2\Omega_0$ by Equation (47a) and hence by Equation (48) there is a double lift loss. In general for asymmetrical vortices $y_r \neq y_l$ and/or unequal vorticities $\Omega_r \neq \Omega_l$, and f satisfying Equation (49) can be found using f_r in Equation (27) and a similar expression for f_l. Substituting Equation (48) in Equation (46) the vertical acceleration in shown to be:

$$m_2\ddot{z} = -\frac{2f}{1+\lambda} C_{L_\alpha} \rho U_2 S_2 \frac{a}{b_2} a\Omega_+(t) \qquad \ldots (50)$$

where the index '2' refers to the following aircraft (it is omitted in $f_2 \equiv f$ because it only appears for the following aircraft).

Substitution of the vorticity Equation (45) in Equation (50) leads to the downward acceleration:

$$\ddot{z} = -g \frac{C_{L_\alpha}}{2\pi} \frac{2f}{1+\lambda} \frac{W_1}{W_2} \frac{S_2}{S_1} \frac{U_2}{U_1} \frac{a}{b_2} \frac{c_{r_1} a}{\eta t} \exp\left(-\frac{a^2}{2\eta t}\right) \qquad \ldots (51)$$

which shows the following dependences:

(*i*) the proportionality to the acceleration of gravity gives the right dimensions, the minus sign indicates downward acceleration and all the following factors are dimensionless;
(*ii*) the next factor is the ratio of the lift slope C_{L_α} to the value 2π for a Joukowsky airfoil;
(*iii*) the following factor involves the taper ratio of the wing of the following aircraft λ, and the geometry of the encounter through f where the latter depend on the former through Equation (27);
(*iv*) the downward acceleration increases for a heavier aircraft leading a lighter aircraft, and larger wing area of the following aircraft relative to the leading aircraft, because a leading aircraft with higher wing loading W_1/S_1 creates a stronger wake, and a following aircraft with smaller wing loading W_2/S_2 is more susceptible to the wake;
(*v*) the downward acceleration increases for slower leading aircraft (which has stronger wake by Equation (40)) and faster following aircraft (which catches the wake sooner, before it has decayed more and has a larger dynamic pressure effect);
(*vi*) the downward acceleration is proportional to the ratio of the vortex radius to wing span, i.e. larger if the vortex covers a larger fraction of the span;
(*vii*) the downward acceleration at the following aircraft is also proportional to the root chord of the wing of the leading aircraft [which appears in the vortex strength Equation (44)], to the vortex radius, and is inversely proportional to the viscosity, because a smaller viscosity implies a slower decay of vorticity and a stronger wake effect;
(*viii*) the downward acceleration depends on time, being initially zero $\ddot{z} = 0$, for $t = 0$, since the flow is potential at the trailing edge of the leading aircraft, then increases due to the roll-up of the trailing vortices, and when viscosity dominates causing vortex decay, then $\ddot{z}$ decreases again with time. The normal separation distances are, of course, far from the peak vorticity, and into the region of vortex decay.

The roll acceleration

$$I\ddot{\phi} = R \qquad \ldots (52)$$

is due to the rolling moment Equation (29) where as in Equation (46) a linear uncoupled response is assumed, for the initial stages of the disturbance following the vortex encounter. This linear response

https://doi.org/10.1017/S0001924000000154 Published online by Cambridge University Press

applies at least up to a bank angle $\phi = 10°$, which is the airline rule of a mandatory go-round in case of a wake vortex encounter on approach to land. For a short time, damping effects are also neglected. For identical vortex core radii, it is given by:

$$\iota_r = a_l \equiv a: \quad R = -\frac{C_{L_\alpha} \rho U S}{1+\lambda} a^2 h \Omega_- (t) \qquad \ldots (53)$$

where the average encounter factor for the rolling moment h is defined by:

$$\Omega_r h_r - \Omega_l h_l \equiv (\Omega_r - \Omega_l) h = 2h\Omega_- \qquad \ldots (54)$$

In the case of symmetric vortices $y_r = -y_l$, since $h_r = h_l$ by Equation (30) then Equation (54) is an identity, taking into account Equation (47b); in the particular case of symmetrical vortices $h_r = h_l$ and opposite vorticities $\Omega_r = \Omega_l$ then $\Omega_r h_r - \Omega_l h_l = 0$ there is no rolling moment; in the general case of asymmetrical vortices $y_r \neq -y_l$ and of dissimilar vorticities $y_r \neq -y_l$ the condition Equation (54) specifies h, in terms of h_r Equation (30) and h_l. Substitution of Equation (54) in Equation (52) yields:

$$I_2 \ddot{\phi} = -\frac{2 C_{L_\alpha} h}{1+\lambda} \rho U_2 S_2 a^2 \Omega(t) \qquad \ldots (55)$$

Using Equation (45) for the vorticity dependence on time, for wing tip vortices with the same radius, leads to:

$$I_2 \ddot{\phi} = -\frac{2h}{1+\lambda} \frac{U_2}{U_1} \frac{S_2}{S_1} W_1 a \frac{c_{r_1} a}{\eta t} \exp\left(-\frac{a^2}{2\eta t}\right) \qquad \ldots (56)$$

where the index '1' refers to the leading aircraft and the index '2' refers to the following aircraft. The radius of gyration in the roll axis of the following aircraft is defined by:

$$I_2 = m (r_2)^2 = W_2 (r_2)^2 / g \qquad \ldots (57)$$

as the distance r_2 from the axis of which the mass m_2 of the aircraft would have to be concentrated to produce the same moment of inertia I_2 as the distributed mass of the real aircraft.

Substituting Equation (57) in Equation (56), the roll acceleration is given by:

$$\ddot{\phi} = -\frac{g}{a} \frac{C_{L_\alpha}}{2\pi} \frac{2h}{1+\lambda} \frac{W_1}{W_2} \frac{U_2}{U_1} \frac{S_2}{S_1} \left(\frac{a}{r_2}\right)^2 \frac{c_{r_1} a}{\eta t} \exp\left(-\frac{a^2}{2\eta t}\right) \qquad \ldots (58)$$

which shows similar dependences as the downward acceleration Equation (51) with three differences:

(*i*) the first factor is g/a to give the correct dimensions of angular acceleration instead of linear acceleration g, by dividing the latter by the vortex core radius;
(*ii*) the square of the vortex radius a^2 is divided by the square of the rolling radius of gyration $(r_2)^2$ in the roll acceleration, instead of the vortex radius a divided by span b_2 in the downward acceleration;
(*iii*) the dependence on the taper ratio λ is the same as in the downward acceleration Equation (51), with f in Equation (49) replaced by h in Equation (54).

The point (*ii*) above lead to the following remark: placing the vortices further outboard (larger a) increases both the vertical Equation (51) and roll Equation (58) accelerations, with the vertical acceleration being larger for smaller span (i.e. vortex further outboard relative to the span), and the roll acceleration being larger for smaller radius of gyration (i.e. vortex further outboard relative to the radius of gyration). The former effect (on vertical acceleration) is linear and the latter (on roll acceleration) is quadratic.

6.0 SINK SPEED AND ROLL RATE

The exponentials in Equation (51) and Equation (58) suggest the introduction of a dimensionless time , which is the ratio of time t to the time $a^2/2\eta$ of peak vorticity of a vortex of core radius a due in the presence of the turbulent viscosity η in Equation (59a):

$$\tau \equiv \frac{2\eta t}{a^2}; \quad \frac{d^2 z}{d\tau^2} = \left(\frac{a^2}{2\eta}\right)^2 \ddot{z} \qquad \ldots (59a,b)$$

using the dimensionless time in the downward acceleration Equation (59b) and (51) leads to:

$$\frac{\mathrm{d}^2 z}{\mathrm{d}\tau^2} = -\frac{f}{1+\lambda} \frac{C_{L_\alpha}}{2\pi} \frac{W_1}{W_2} \frac{S_2}{S_1} \frac{U_2}{U_1} \frac{a}{b_2} \frac{g c_{r_1} a^2}{\eta^2} \frac{a}{\tau} \exp\left(-\frac{1}{\tau}\right) \qquad \ldots (60)$$

next is introduced a dimensionless altitude divided by the vortex radius Equation (61a):

$$X \equiv \frac{z}{a}, \quad A \equiv -\frac{f}{1+\lambda} \frac{C_{L_\alpha}}{2\pi} \frac{W_1}{W_2} \frac{S_2}{S_1} \frac{U_2}{U_1} \frac{a}{b_2} \frac{g c_{r_1} a^2}{\eta^2} \qquad \ldots (61a,b)$$

and the dimensionless factor Equation (61b), so that the roll response equation takes the dimensionless form:

$$\frac{\mathrm{d}^2 X}{\mathrm{d}\tau^2} = \frac{A}{\tau} \exp\left(-\frac{1}{\tau}\right) \qquad \ldots (62)$$

The same transformations Equation (59b) may be applied to Equation (58) the roll acceleration

$$\frac{\mathrm{d}^2 \phi}{\mathrm{d}\tau^2} = -\frac{h}{1+\lambda} \frac{C_{L_\alpha}}{2\pi} \frac{W_1}{W_2} \frac{U_2}{U_1} \frac{S_2}{S_1} \left(\frac{a}{r_2}\right)^2 \frac{g c_{r_1} a^2}{\eta^2} \frac{1}{\tau} \exp\left(-\frac{1}{\tau}\right) \qquad \ldots (63)$$

leads to the same dimensionless form Equation (62) for the bank angle ϕ, which is dimensionless Equation (64a):

$$X \equiv \phi, \quad A \equiv -\frac{h}{1+\lambda} \frac{C_{L_\alpha}}{2\pi} \frac{W_1}{W_2} \frac{U_2}{U_1} \frac{S_2}{S_1} \left(\frac{a}{r_2}\right)^2 \frac{g c_{r_1} a^2}{\eta^2} \qquad \ldots (64a,b)$$

using the dimensionless constant Equation (64b). Since the downward acceleration Equation (61a) and the roll acceleration Equation (64a) satisfy the same dimensionless equation Equation (62), apart from the constant A [respectively Equation (61b) and Equation (64b)], its integration will specify the sink speed and roll rate.

The integration of the dimensionless response for the acceleration Equation (62) specifies the dimensionless velocity change between dimensionless times τ_1 e τ_2:

$$\frac{\mathrm{d}X}{\mathrm{d}\tau} = A \int_{\tau_1}^{\tau_2} \frac{e^{-1/\tau}}{\tau} \mathrm{d}\tau \qquad \ldots (65)$$

A change of variable:

$$T \equiv 1/\tau: \quad \frac{\mathrm{d}X}{\mathrm{d}\tau} = A \int_{T_2}^{T_1} \frac{e^{-T}}{T} \mathrm{d}T \qquad \ldots (66)$$

leads to[8] the exponential integral:

$$E(\xi) \equiv \int_{\xi}^{+\infty} \frac{e^{-T}}{T} \mathrm{d}T \qquad \ldots (67)$$

so that the dimensionless velocity is specified:

$$\frac{\mathrm{d}X}{\mathrm{d}\tau} = A\left[E(1/\tau_2) - E(1/\tau_1)\right] \qquad \ldots (68)$$

https://doi.org/10.1017/S0001924000000154 Published online by Cambridge University Press

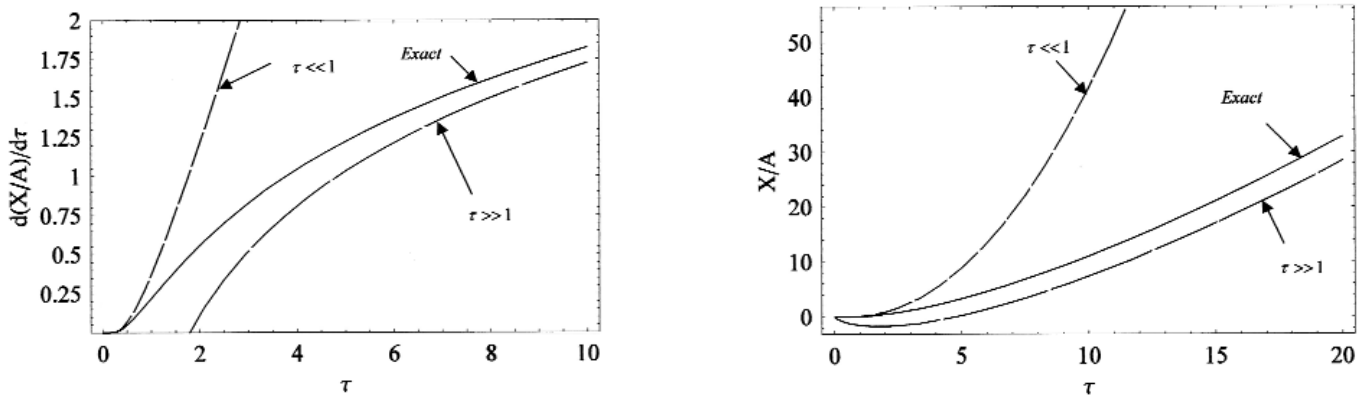


Figure 4. Dimensionless sink rate and roll rate (top) and altitude and bank angle (bottom) versus dimensionless time.

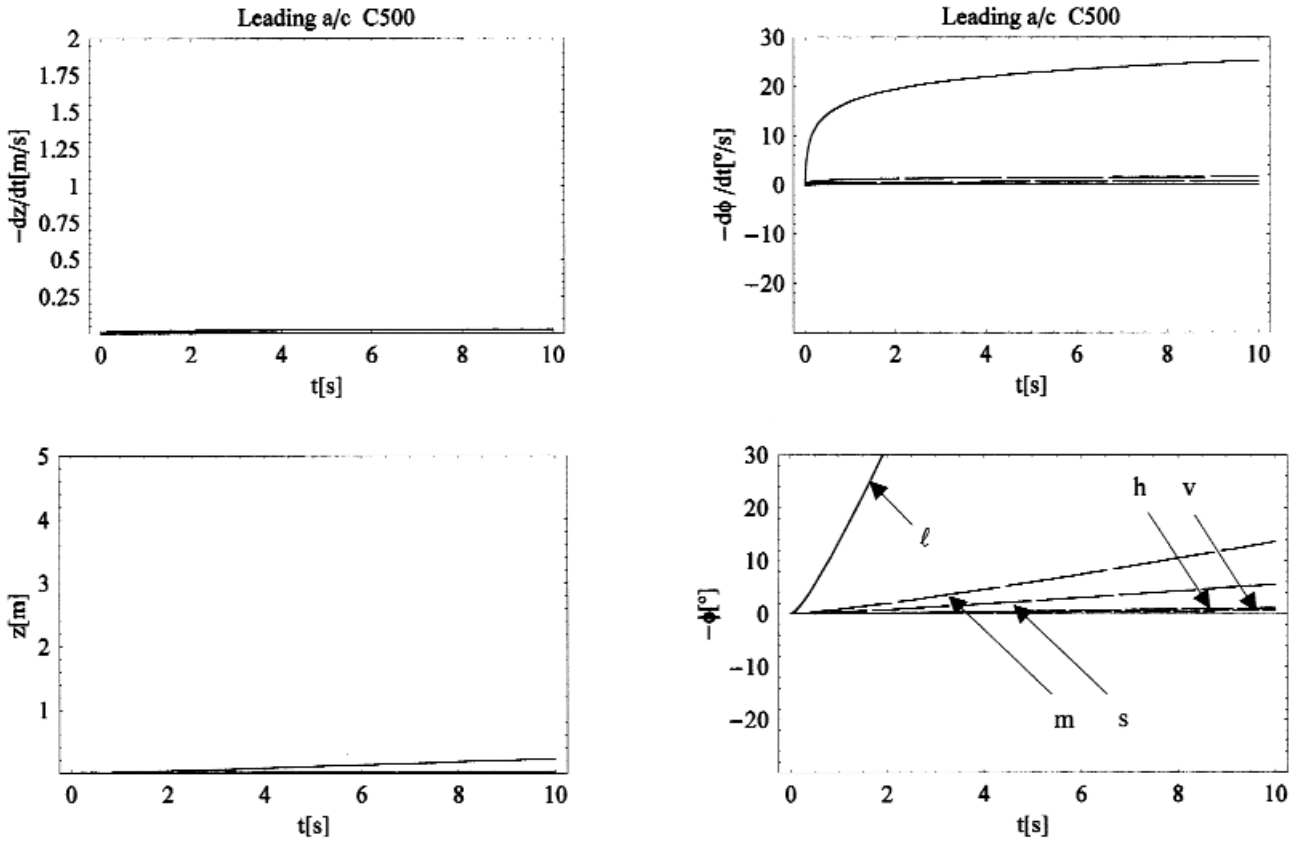


Figure 5. Sink rate (top left), altitude loss (bottom left), roll rate (top right) and bank angle (bottom right), as function of time versus time for light leading aircraft, followed by very large, heavy, special, medium and light aircraft.

$$\frac{dX}{d\tau} = A\left[E(T_2) - E(T_1)\right] \qquad \ldots (69)$$

by the difference of two exponential integrals. If the starting time is taken to be that of the formation of the vortex at the trailing edge of the wing of the leading aircraft, then

$$\tau_1 = 0, \quad T_1 = \infty, \quad E(T_1) = 0 \qquad \ldots (70)$$

and only one exponential integral appears in the dimensionless velocity:

$$\tau_1 = 0, \quad \tau_2 = \tau: \quad \frac{dX}{d\tau} = AE(1/\tau) \qquad \ldots (71)$$

The exponential integral is specified[8] by the series for large τ:

$$A^{-1}\frac{dX}{d\tau} = -\gamma + \ln\tau - \sum_{n=1}^{\infty}\frac{(-1)^n}{n}\frac{\tau^{-n}}{n!} \qquad \ldots (72)$$

where γ = 0·57721... is Euler's constant; it diverges for $\tau = \infty$, implying that the encounter of the entire vortex would leads to an

https://doi.org/10.1017/S0001924000000154 Published online by Cambridge University Press

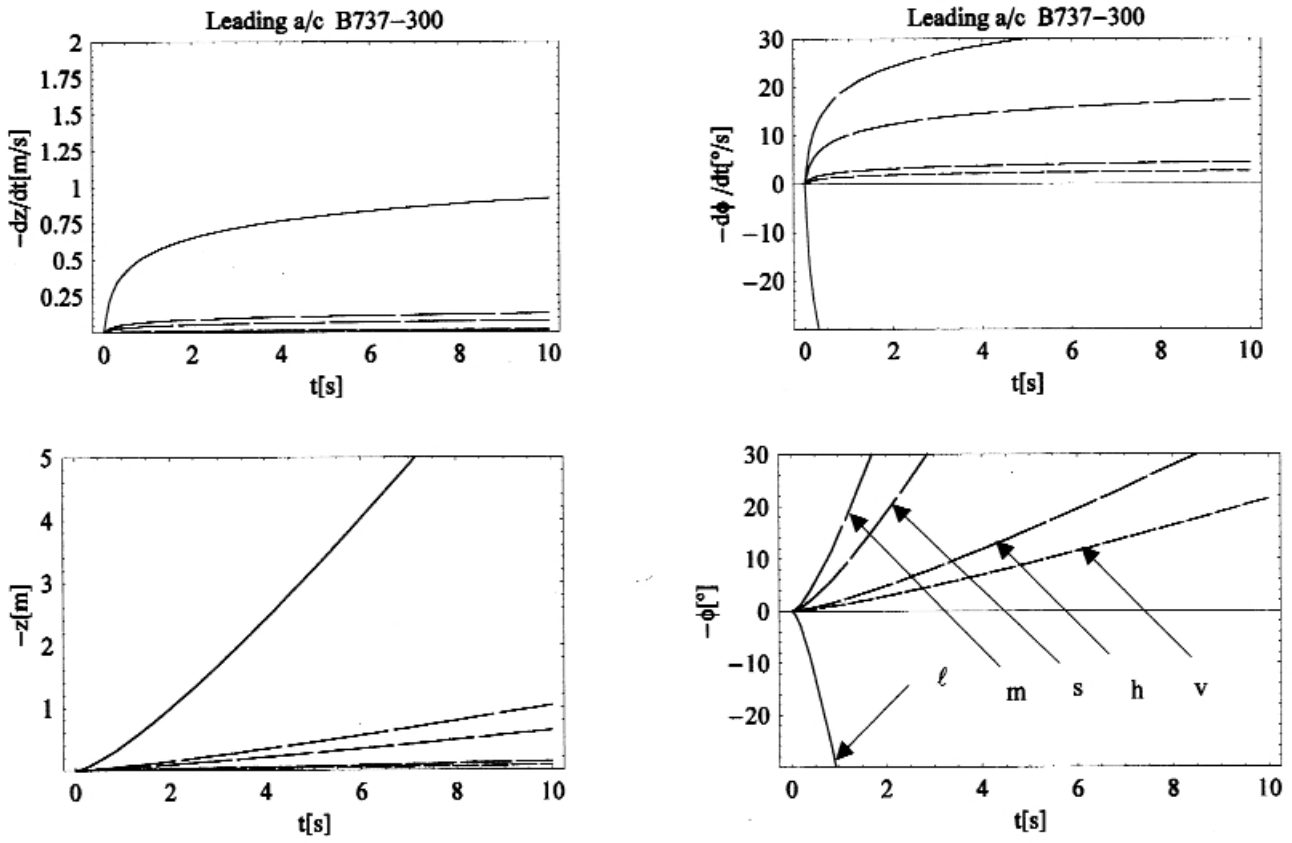


Figure 6. As Fig. 5 for medium leading aircraft.

infinitive dimensionless velocity. In practice, the interaction of the wake of the leading aircraft with the following aircraft takes a finite time. For small , the asymptotic formula[8] for the exponential integral should be substituted in Equation (71), *viz*

$$\frac{\mathrm{d}X}{\mathrm{d}\tau} = A\tau e^{-1/\tau}\left(1-\tau+2\tau^2-6\tau^3+24\tau^4-\ldots+(-1)^n n!\tau^n+\ldots\right) \quad \ldots (73)$$

The transformation from dimensionless time Equation (59a) to time:

$$\frac{\mathrm{d}X}{\mathrm{d}t} = \frac{2\eta}{a^2}\frac{\mathrm{d}X}{\mathrm{d}\tau} \quad \ldots (74)$$

specifies the dimensional velocity from the dimensionless one. Substituting Equation (59a) and (63) in Equation (71) the rate equation is:

$$\frac{\mathrm{d}X}{\mathrm{d}t} = \frac{2\eta}{a^2}AE\left(\frac{a^2}{2\eta t}\right) \quad \ldots (75)$$

Using Equation (61a,b) leads to the sink speed:

$$\dot{z} = BE\left(\frac{a^2}{2\eta t}\right) \quad \ldots (76a)$$

where the constant Equation (76b) is given by

$$B = -\frac{2f}{1+\lambda}\frac{C_{L_\alpha}}{2\pi}\frac{W_1}{W_2}\frac{S_2}{S_1}\frac{U_2}{U_1}\frac{a}{b_2}\frac{gc_{r_1}a}{\eta} \quad \ldots (76b)$$

Using Equation (73) for short time shows that the sink speed

$$t << a^2/2\eta \equiv t_*: \quad \dot{z} = -\frac{4f}{1+\lambda}\frac{C_{L_\alpha}}{2\pi}\frac{W_1}{W_2}\frac{S_2}{S_1}\frac{U_2}{U_1}\frac{gc_{r_1}t}{b_2}\exp\left(-\frac{a^2}{2\eta t}\right) \quad \ldots (77)$$

has the same dependence as the downward acceleration Equation (51), except that the factor $a/\eta t$ in the latter is replaced by $2t/a$ in Equation (77). Substituting Equation (64a,b) in Equation (75) leads to the roll rate:

$$\dot{\phi} = DE\left(\frac{a^2}{2\eta t}\right) \quad \ldots (78a$$

where the constant is given by:

$$D \equiv -\frac{2h}{1+\lambda}\frac{C_{L_\alpha}}{2\pi}\frac{U_2}{U_1}\frac{S_2}{S_1}\frac{W_1}{W_2}\left(\frac{a}{r_2}\right)^2\frac{c_{r_1}g}{\eta} \quad \ldots (78b)$$

For short time Equation (73) can be used to specify the roll rate.

$$t << a^2/2\eta \equiv t_*: \quad \dot{\phi} = -\frac{4h}{1+\lambda}\frac{C_{L_\alpha}}{2\pi}\frac{W_1}{W_2}\frac{U_2}{U_1}\frac{S_2}{S_1}\frac{c_{r_1}}{r_2}\frac{gt}{r_2}\exp\left(-\frac{a^2}{2\eta t}\right) \quad \ldots (79)$$

which scales like the roll acceleration Equation (58) with $a/\eta t$ replaced by $2t/a$ in Equation (79). The results Equation (77) and (79) would apply for a time short compared with the wing tip vortex roll-up time $t << a^2/2\eta \equiv t$ whereas the cases of wake vortex encounters correspond to much longer times $t >> t$, for which Equation (76a) and (78a) should be used and are included in the plots in Figs 3 to 9. The preceding formulas specify the sink speed and roll rate respectively, and by integration, the altitude loss and bank angle.

https://doi.org/10.1017/S0001924000000154 Published online by Cambridge University Press

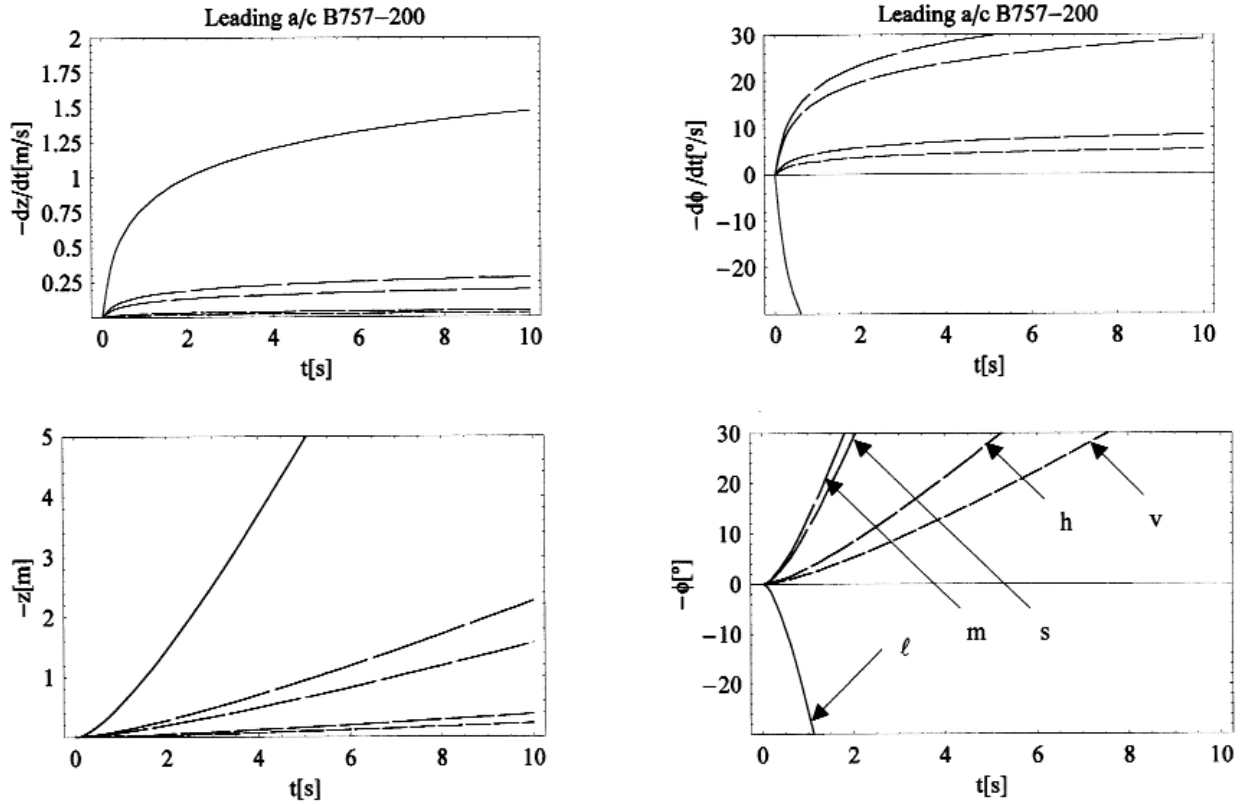


Figure 7. As Fig. 5 for special leading aircraft.

Table 1
The five classes of aircraft, *viz* the three ICAO categories plus special and very large, with their symbols, and the examples chosen for the response plots in Figs 4 to 8

Designation	Symbol	Example	Leading in
ICAO: light	ℓ	Cessna Citation 500	Figure 5
ICAO: medium	m	Boeing 737-700	Figure 6
special	s	Boeing 757-200	Figure 7
ICAO: heavy	h	Boeing 747-400	Figure 8
very large	v	VLTA	Figure 9

7.0 ALTITUDE LOSS AND BANK ANGLE

It has been shown that the dimensionless altitude Equation (61a) and the roll angle Equation (64a) satisfy the same acceleration equation Equation (62), in terms of the dimensionless time Equation (59a), where the difference appears only in the constant A, which is specified by Equation (61b) for the altitude and by Equation (64b) for the roll angle. It follows that the dimensionless sink speed and roll rate satisfy the same equation Equation (71), *viz*:

$$\frac{\mathrm{d}}{\mathrm{d}\tau}\left(\frac{X}{A}\right) = E\left(\frac{1}{\tau}\right) \qquad \ldots (80)$$

whose exact solution is plotted as the solid line on the left-hand panel of Fig. 4, in comparison with:

(*i*) the approximation Equation (73) for short dimensionless time $\tau << t$, plotted as a line with long dashes;
(*ii*) the approximation Equation (74) for long dimensionless time $\tau >> t$, plotted as a line with short dashes.

It is clear that the short time approximation is of very inaccurate except very near the origin; the long time approximation is more useful, but still gives errors of about 10% for $\tau = 8$. A further integration for the dimensionless altitude or roll angle X/A as a function of the dimensionless time, shows on the right-hand panel of Fig. 4, a similar situation. The short time approximation (dashed line) diverges from the exact solution (thin solid line) for rather short dimensionless time $\tau << 1$, and it takes a long dimensionless time $\tau >> 8$ for the long time approximation (thin solid line) to represent accurately the exact solution. It follows that it is safer to use the exact solution, at least in the range $0{\cdot}5 < \tau < 6$; this is not difficult, since the exponential integral is tabulated[8], and it is a smooth function allowing accurate numerical integration over finite intervals.

In order to apply the preceding results in numerical form, example aircraft are chosen, in each of the five categories indicated in Table 1:

(*i*) the light, medium and heavy categories correspond to the ICAO classification by maximum take-off weight, for the purpose of setting separation distances;
(*ii*) the Boeing 757-200 has been added as a 'special' aircraft class since after several incidents, the FAA has decided it requires larger separation than other aircraft in its weight category;
(*iii*) a very large transport aircraft (VLTA) has been added as a 'very large' class, to represent future airliners significantly larger than the Boeing 747-400, to assess whether they would justify the creation of an additional ICAO or FAA category 'super-heavy'.

https://doi.org/10.1017/S0001924000000154 Published online by Cambridge University Press

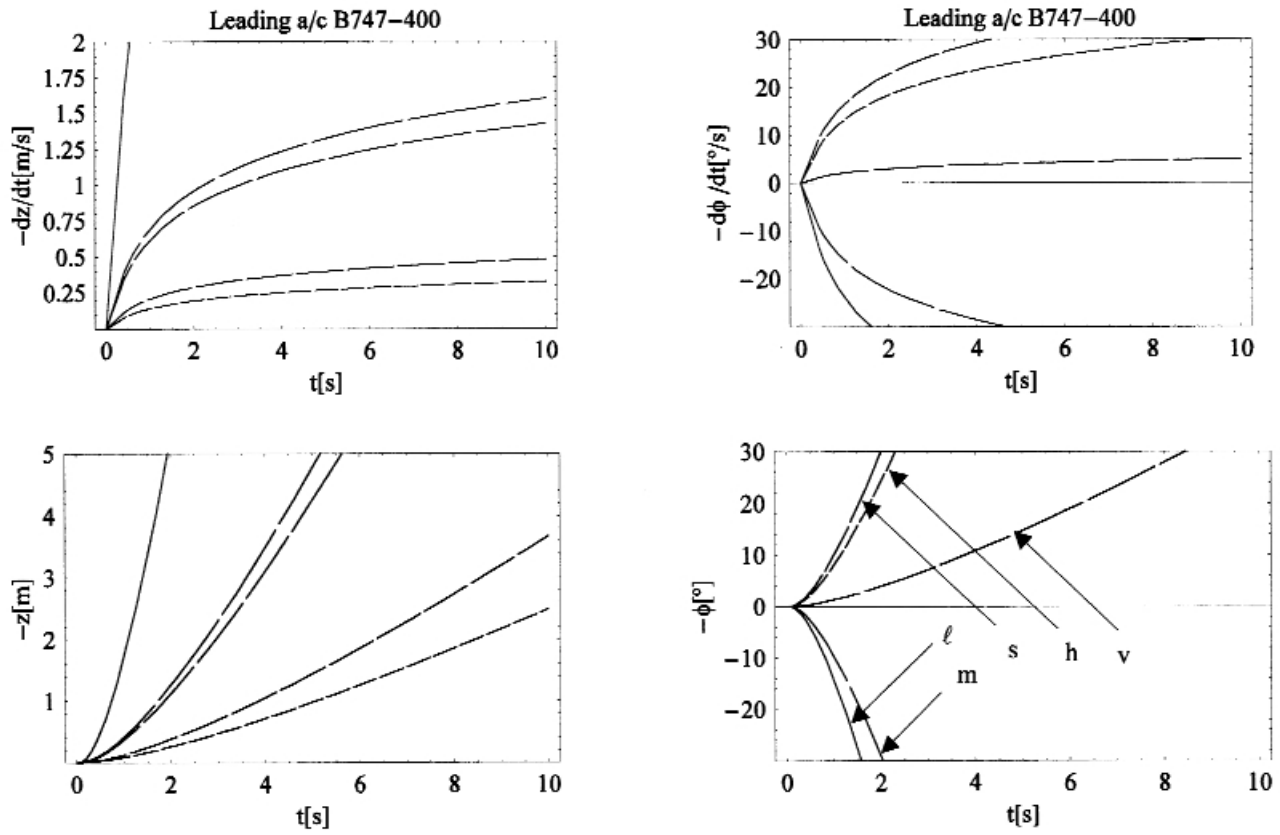


Figure 8. As Fig. 5 for heavy leading aircraft.

The data on each of the chosen aircraft in the five classes 'light', 'medium', 'heavy', 'special' and 'very large' (subscripts respectively $\boldsymbol{\ell}$, m, h, s, v), is listed in Table 2, consisting of manufacturers' data from open sources[21,22] in the upper part, and data calculated from the former in the lower part. The required manufacturers' data is the maximum landing weight W, the wing area S and the span b, the tip chord c_r, the rolling radius of gyration r and the approach speed for landing U. From these are calculated the geometric mean chord $\bar{c} = S/b$, the root chord $c_r = 2\bar{c} - c_t$ by Equation (8b), the taper ratio Equation (8a), the vortex core radius $a = 0{\cdot}05b_1$ for the Hallock-Burham vortex model and the wake vortex circulation strength Equation (44). The two wing tip vortices were assumed to have equal core radii $a_r = a_l = a$, and the separation between the wing tip vortices of the leading aircraft to reduce to $b_1/\pi = 0{\cdot}318b_1$; also, it is assumed (Fig. 2) that the following aircraft flies parallel to the leading aircraft offset a distance $y_0 = -b_2/8 = -0125b_2$ to the left. With five classes of aircraft, there are 25 leader-follower combinations in Table 3, for which are indicated the following additional lateral distances, relative to the centreline of the following aircraft:

(*i*) the axis of the right y_r and left y_l vortices:

$$y_r, y_l = \pm b_1/\pi - b_2/8 = -0{\cdot}125\ b_2 \pm 0{\cdot}318\ b_1 \quad \ldots (81a,b)$$

(*ii*) the upper y^+ and lower y^- limits of the span of the following aircraft covered by the cores of the right $y_r^{\pm}$ and left $y_l^{\pm}$ vortices:

$$y_r^{\pm} = y_r \pm a_r = b_1/\pi - b_2/8 \pm 0{\cdot}05\ b_1 = -0{\cdot}125 b_2 + {}^{0{\cdot}368}_{0{\cdot}268}\ b_1 \ldots (82a,b)$$

$$y_l^{\pm} = y_l \pm a_l = -b_1/\pi - b_2/8 \pm 0{\cdot}05 b_1 = -0{\cdot}125 b_2 - {}^{0{\cdot}268}_{0{\cdot}368}\ b_1 \ldots (83a,b)$$

(*iii*) the right b_r and left b_l wing tip positions of the leading aircraft relative to the following aircraft:

$$b_r, b_l = y_0 \pm b_1/2 = -b_2/8 \pm b_1/2 = -0{\cdot}125\ b_2 \pm 0{\cdot}500\ b_1 \quad \ldots (84a,b)$$

Table 3 indicates which of the positions fall within the span $|y| \le b_2/2$ of the following aircraft, and thus specifies the wake vortex encounter geometry.

The 25 combinations are illustrated in Figs 5 to 9 respectively for light ($\boldsymbol{\ell}$), medium (m), special (s), heavy (h) and very large (v) aircraft leading; in each figure the five classes of following aircraft are considered, *viz* v, h, s, m, $\boldsymbol{\ell}$. Each figure consists of four panels, with sink rate (top) and altitude loss (bottom) on the left-hand side and roll rate (top) and bank angle (bottom) on the right-hand side. For a leading light aircraft (Fig. 5), the sink speed (top right) and altitude loss (bottom right) are quite small, which is quite noticeable since the same scale $0 \le dz/dt \le 5\text{ms}^{-1}$ and $0 \le z \le 5m$ has been taken for the plots for all 25 encounters in Figs 5 to 9; although the same scale has been taken also (top left) for roll rate $|d\phi/dt| \le 30°\text{s}^{-1}$ and (bottom left) bank angle $|\phi| \le 30°$, the roll response to a light leading aircraft is visible, and more pronounced for a light following aircraft. If a medium aircraft is leading (Fig. 6), the sink rate (top right) and altitude loss (bottom right) are noticeable for a light following aircraft, and the roll rate (top left) and bank angle (bottom left) show significant response, except for the heavy and large aircraft. A light aircraft following a medium aircraft rolls in opposite direction to all other four classes of following aircraft, because it catches only one

https://doi.org/10.1017/S0001924000000154 Published online by Cambridge University Press

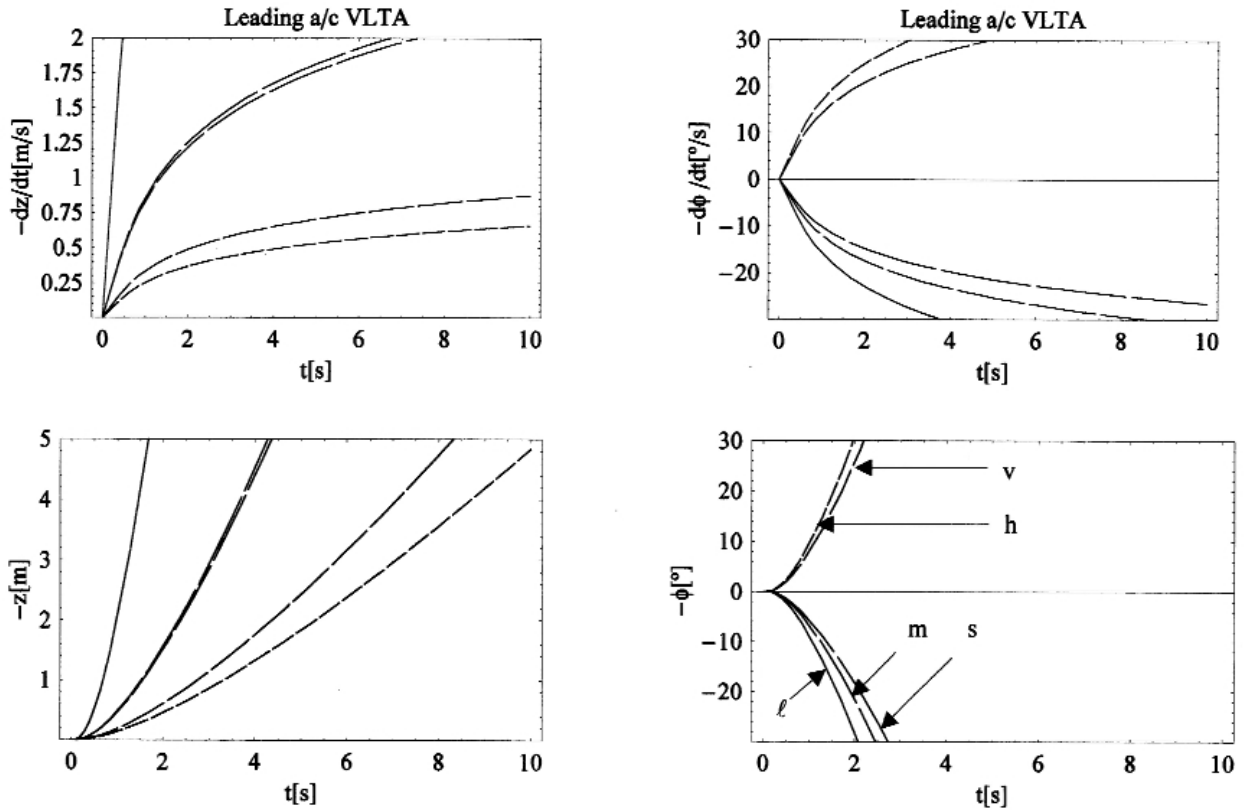


Figure 9. As Fig. 5 for very large leading aircraft.

Table 2
Aircraft data needed for response calculation, starting with basic data (top) and completed with derived data (bottom)

Category symbol	Index unit	ℓ C500	m B737-300	s B757-200	h B747-400	v VLTA
W	kg	4,400	51,720	89,810	260,360	381,000
S	m^2	22·3	105·41	185·25	520·03	920
b	m	14·26	28·88	38·05	64·44	79·8
c_t	m	0·8	1	1·47	1·5	3·87
r	m	1·7825	4·332	6·7729	11·5992	14·763
U	ms^{-1}	54·9	60	70·6	60	60
$\overline{c}$	m	1·56	3·65	4·87	8·07	11·52
c_r	m	2·33	6·3	8·27	14·64	19·16
λ	-	0·343	0·159	0·178	0·102	0·202
a	m	0·713	1·444	1·903	3·222	3·99
Γ_0	m^2s^{-1}	63·5	330	430	707	859

vortex from the leading aircraft, *viz* that coming from the right wing tip, as can be checked from the entry m-ℓ in Table 3. The case of special leading aircraft (Fig. 7) shows smaller response for the heavy and large following aircraft, and increasing response for the special, medium and light aircraft, with the light aircraft rolling in opposite directions to all others, for the same reason of catching only one wing tip vortex from the leading aircraft. The case of heavy leading aircraft (Fig. 8) causes significant response in all following aircraft except the large, and now the light and medium following aircraft roll in opposite direction to the other three classes. The large leading aircraft (Fig. 9) causes the largest response in the following aircraft, with the light, medium and special rolling in opposite direction to the heavy and large following aircraft.

https://doi.org/10.1017/S0001924000000154 Published online by Cambridge University Press

Table 3
Spanwise location relative to following aircraft, of the axis of the leading aircraft, and position of its wings tips and wing tip vortices, using the values and notation of Fig. 2.

Leading	Following	$-\frac{b_2}{2}$	b_l	y_l^-	y_l	y_l^+	y_0	y_r^-	y_r	y_r^+	b_r	$+\frac{b_2}{2}$
	ℓ	–7	–9	–7	–6	–6	–2	2	2·8	3	5·3	7
	m	–14	–18	–9	–8	–7	–4	0	0·9	2	11	14
ℓ	*s*	–19	–24	–10	–9	–9	–5	–1	–0	0	14	19
	h	–32	–40	–13	–13	–12	–8	–4	–4	–3	24	32
	v	–40	–50	–15	–15	–14	–10	–6	–5	–5	30	40
	ℓ	–7	–9	–12	–11	–10	–2	6	7·4	9	5·3	7
	m	–14	–18	–14	–13	–11	–4	4	5·6	7	11	14
m	*s*	–19	–24	–15	–14	–13	–5	3	4·4	6	14	19
	h	–32	–40	–19	–17	–16	–8	–0	1·1	3	24	32
	v	–40	–50	–21	–19	–18	–10	–2	–1	1	30	40
	ℓ	–7	–9	–16	–14	–12	–2	8	10	12	5.3	7
	m	–14	–18	–18	–16	–14	–4	7	8·5	10	11	14
s	*s*	–19	–24	–19	–17	–15	–5	5	7·4	9	14	19
	h	–32	–40	–22	–20	–18	–8	2	4·1	6	24	32
	v	–40	–50	–24	–22	–20	–10	0	2·1	4	30	40
	ℓ	–7	–9	–26	–22	–19	–2	16	19	22	5·3	7
	m	–14	–18	–27	–24	–21	–4	14	17	20	11	14
h	*s*	–19	–24	–28	–25	–22	–5	13	16	19	14	19
	h	–32	–40	–32	–29	–25	–8	9	12	16	24	32
	v	–40	–50	–34	–30	–27	–10	7	11	14	30	40
	ℓ	–7	–9	–31	–27	–23	–2	20	24	28	5·3	7
	m	–14	–18	–33	–29	–25	–4	18	22	26	11	14
v	*s*	–19	–24	–34	–30	–26	–5	17	21	25	14	19
	h	–32	–40	–37	–33	–29	–8	13	17	21	24	32
	v	–40	–50	–39	–35	–31	–10	11	15	19	30	40

Table 4
Time to reach 10° bank angle for all 25 combinations of leading and following aircraft in the five categories *ℓ*, *m*, *h*, *s*, *v*, in agreement with bottom left plots in Figs 5 to 9

Leading / Following	*ℓ*	*m*	*s*	*h*	*v*
ℓ	0·798	0·438	0·544	0·818	1·090
m	7·683	0·770	0·847	1·028	1·398
s	16·50	1·253	0·945	3·807	1·270
h	66·38	3·537	2·284	1·013	1·147
v	114·3	5·393	3·232	1·153	1·040

8.0 WAKE RESPONSE AND GO-ROUND CRITERIA

The Table 4 indicates, for all 25 combinations of five classes of leading and following aircraft, the time in seconds to reach a bank angle of $\phi = 10°$; this value is chosen because it is the airline criterion for a mandatory go-round, in the case of a wake vortex encounter on approach to land. The times to ten-degree bank angle listed in Table 4 can be read-off the bottom right panel of Figs 5 to 9, which indicate bank angle response. A bank angle of ten degrees is reached quickly, for a light leading aircraft, only if the following aircraft is also light; as the leading aircraft moves up the scale, to medium, special, heavy and large, so the times to ten-degree bank angle become short for more classes of following aircraft. In the case of heavy or large leading aircraft, the times to ten-degree bank angle are short and of the order of one second for all classes of following aircraft. The exception of slower response for a special aircraft following a heavy, is a special case (bottom left of Fig. 8) of a following aircraft on the 'borderline' between those rolling to the right and those rolling to the left; this means that the wing tip vortices from the leading aircraft hit the following aircraft at an asymmetric position which happens to produce a smaller rolling moment. The opposite case, of very quick roll (seen on bottom left panels of Figs 5 to 9) is that of a smaller following aircraft catching only one wing tip vortex from a bigger leading aircraft.

The conclusions both from Figs 5 to 9 and Table 4 are:

(*i*) the roll response is more significant for bigger leading aircraft (in the scale light, medium, special, heavy and large), and smaller following aircraft;
(*ii*) the roll response may be reduced in cases where the two wing tip vortices almost counter each other, but this a fortuitous case which cannot be relied upon;
(*iii*) an unfortunate situation which is certain to increase roll response, is when a smaller following aircraft catches only one wing tip vortex from a bigger leading aircraft.

The Figs 5 to 9 represent an upper bound or a worst case scenario in which the following aircraft will hit the whole vortex from the time of generation, *viz* they concern the response of the following aircraft in the conditions Equation (71), i.e. assuming it experiences the entire time evolution of the wake of the leading aircraft, from the initial potential flow, to the vortex roll-up and subsequently decay due to viscosity.

If only a part of the vortex wake evolution is considered, then Equation (68) must be used, subtracting the term $E(T_1)$ due to the evolution before the time $\tau_1 = 1/T_1$. In Fig. 10 the case of heavy leading aircraft and medium following aircraft is considered with vortex starting times $t_0/t_* = 0, 1, 2, 5, 10$ a multiple of the peak

https://doi.org/10.1017/S0001924000000154 Published online by Cambridge University Press

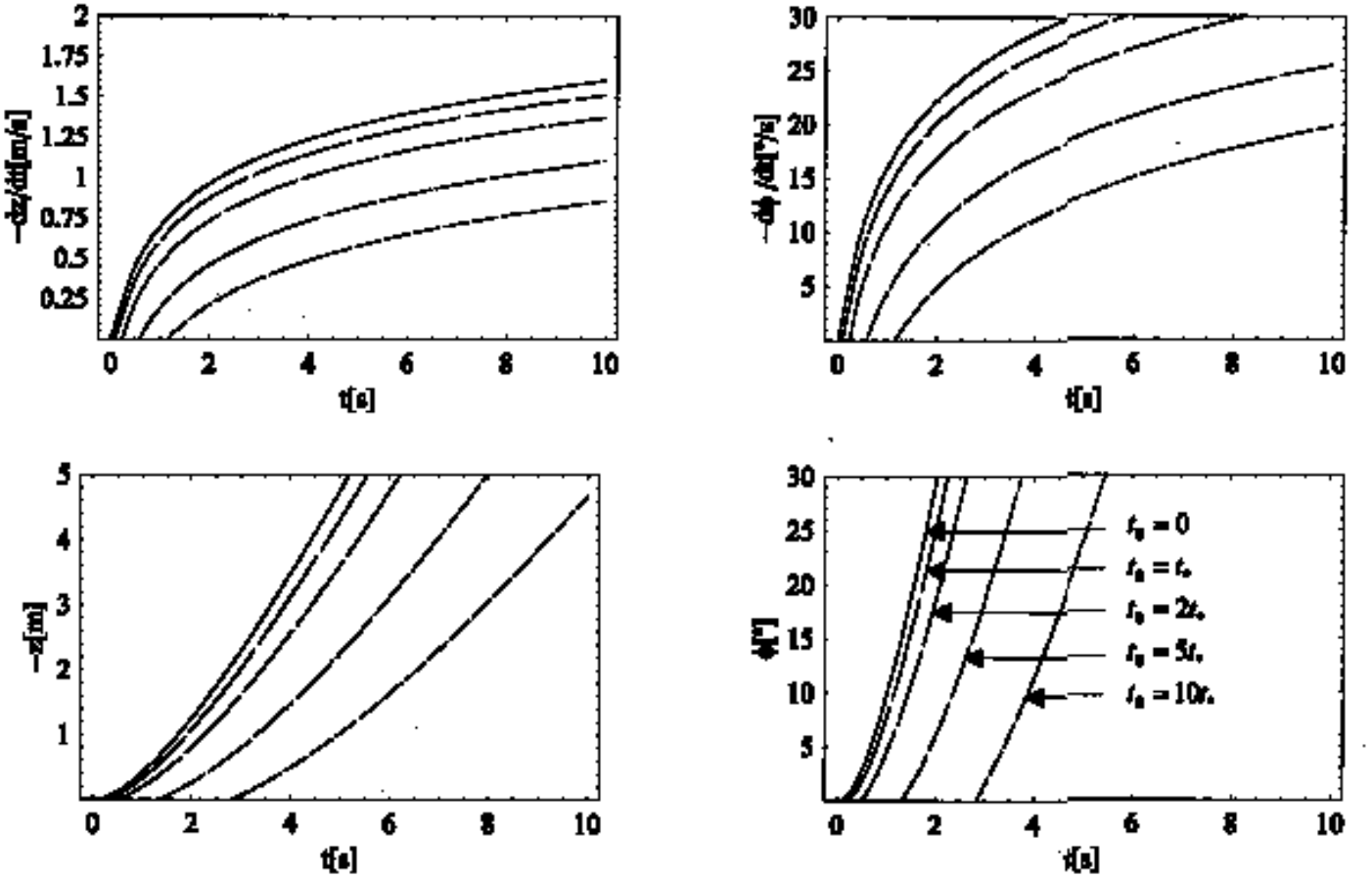


Figure 10. As Fig. 5 for heavy leading aircraft and medium following aircraft, with starting time at a multiple of the peak vorticity time $t_0/t_* = 0,1,2,5,10$.

vorticity time defined as the time t_* when the vorticity Equation (40) is maximum:

$$t_* = a^2 / 2\eta, \quad \Omega_{max} \equiv \Omega(t_*) = \Gamma_0 / \pi a^2 e \qquad \ldots (85a,b)$$

It is seen in Fig. 10 that if the following aircraft encounters the wake vortex of the leading aircraft with greater separation, the induced sink rate (top left) is initially smaller, and thus takes longer (bottom left) to build-up to the same altitude loss; a similar remark can be made with regard to roll rate (top right), which is initially smaller for larger separation distance, although the bank angle (bottom right) still builds-up quite fast.

9.0 DISCUSSION

The vortex wake of the leading aircraft was considered to be the only effect on vertical acceleration Equation (46) and roll acceleration Equation (52) of the following aircraft, thus isolating this aspect, to illustrate better its consequences. It is clear that these results could be extended by including the damping terms, which become important for longer times, in limiting rates e.g. roll or sink rates. Also, the effect of control surface deflections are important in limiting flight deviations, e.g. roll angles and altitude loss. The coupling of vertical acceleration to pitch and longitudinal motions, and the coupling of roll to yaw and sideslip are generally less important[17] than the effects of control surfaces and damping. The encounter geometry considered was very simple, in that the following aircraft flies parallel to the wake of the leading aircraft, staying indefinitely at a constant lateral distance from the axis. In a vortex crossing configuration, the wake effects are more transient, and can lead not to a roll to one side only, but rather to a large wing rock motion. The present theory can be applied to this case, allowing for the vortex position relative to the wing to vary with time, and splitting the vorticity into longitudinal and lateral components, as appropriate. The effect of distinct vortex 'core' and 'external flow' models on the wake vortex encounter is another subject of investigation, but should not alter significantly the results.

The preceding predictions should be substantiated by comparison with experimental data. Since the vorticity decay function Equation (40) is the key element for the calculation of wake effects, its comparison with flight measurements, from the Memphis data base [22-23] is a suitable validation. The vorticity is put in a dimensionless form using the tangential velocity at the vortex core radius Equation (2), *viz*:

$$\bar{\omega} = (a / w(a))\Omega(t) = (4\pi a^2 / \Gamma_0)\Omega(t) \qquad \ldots (86)$$

leading from Equation (40) to:

$$\bar{\omega}(\bar{t}) = (4 / v\bar{t})\exp(-1/v\bar{t}) \qquad \ldots (87)$$

where $\bar{t}$ is a dimensionless time t divided by a time scale t_0 in Equation (88a):

https://doi.org/10.1017/S0001924000000154 Published online by Cambridge University Press

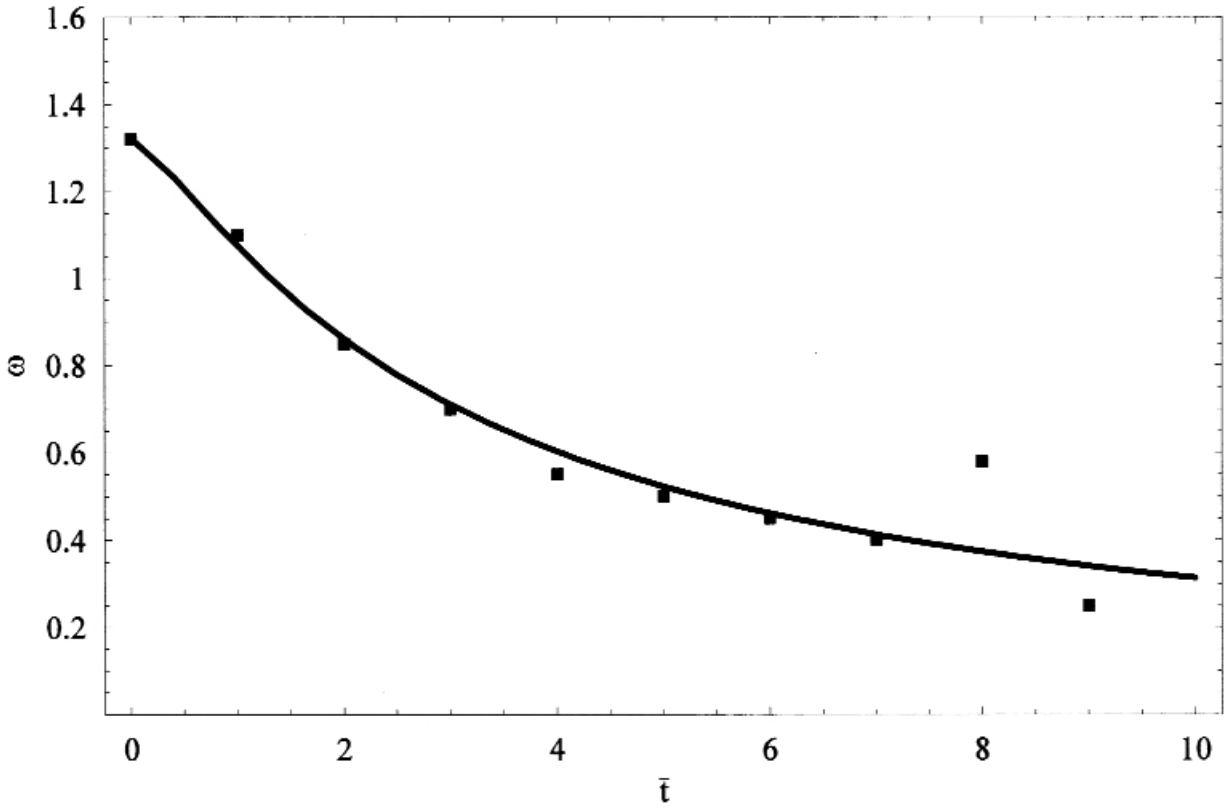


Figure 11. Comparison of the vorticity decay function with Memphis flight test data.

$$\bar{t} \equiv t/t_0\,, \quad \nu \equiv 2\eta t_0/a^2 = t_0/t_* \qquad \ldots (88a,b)$$

and the viscosity is made dimensionless Equation (88b) dividing the time scale t_0 by the time t_* of the peak vorticity Equation (85b). The vortex is not encountered at the time of formation $\bar{t} = 0$, but rather at a later time $\bar{t}_1$, so the substitution $t \to \bar{t}_1 + \bar{t}$ is made in the vorticity Equation (87), *viz*:

$$\omega(\bar{t}) = \bar{\omega}(\bar{t}_1 + \bar{t}) = [4/\nu(\bar{t}_1 + \bar{t})]\exp\{-1/[\nu(\bar{t}_1 + \bar{t})]\} \qquad \ldots (89)$$

for comparison with flight test data.

The comparison of Equation (89) in the form:

$$\omega(\bar{t}) = [C_1/(\bar{t}_1 + \bar{t})]\exp\{-C_2[(\bar{t}_1 + \bar{t})]\} \qquad \ldots (90)$$

with the Memphis records (Fig. 11) shown a good fit for:

$$\bar{t}_1 = 1{\cdot}229\,, \quad C_1 = 3{\cdot}85\,, \quad C_2 = 1{\cdot}06 \qquad \ldots (91a,b,c)$$

Note that the values of C_1 and C_2 are not independent in Equation (87) ≡ Equation (89), *viz*:

$$C_1 = 4/\nu = 4C_2 \qquad \ldots (92)$$

The ratio $C_1/C_2 = 3{\cdot}63$ in Equation (91b,c) shows that the theoretical prediction $C_1/C_2 = 4$ has a moderate error of 10%. Thus the vorticity decay law is validated both quantitatively, and in shape as a function of time (Fig. 11).

ACKNOWLEDGEMENTS

The authors are grateful to the referees for their remarks which contributed to the improvement of the paper. This work has been supported by the project S-Wake of CEC Aeronautics programme and has benefited from comments of other partners in this activity. The second author acknowledges the PhD grant SFRH/BD/3104/2000 from 'Fundação para a Ciência e Tecnologia'.

REFERENCES

1. CAMPOS, L.M.B.C. and MARQUES, J.M.G. On the calculation of safe separation distances between aircraft due to turbulent wakes (in preparation), 2004.
2. SHEN, S., DING, F., HAN, J., LIN, Y-L., ARYA, S.P. and PROCTOR, F.H. Numerical modeling studies of wake vortices: real case simulations, 1999, AIAA Paper 99-0755, 37th Aerospace Sciences Meeting, Reno, Nevada.
3. SPALART, P.R. Airplane trailing vortices, 1998, *Ann Rev Fluid Mech*, **30**, pp 107-138.
4. ROSSOW, V.J. Lift-generated vortex wakes of subsonic transport aircraft, 1999, *Progr Aerosp Sci*, 35, pp 507-660.
5. HINTON, D.A. An Aircraft Vortex Spacing System (AVOSS) for dynamical wake vortex spacing criteria, 1996, 78th Fluid Mechanics Panel & Symposium on the Characterization and modification of wakes from lifting vehicles in fluids, Trondheim, Norway.
6. HINTON, D.A., CHARNOCK, J.K., BAGWELL, D.R. and GRIGSBY, D. NASA aircraft vortex spacing system development status, 1999, AIAA 37th Aerospace Sciences Meeting, Reno, Nevada.

https://doi.org/10.1017/S0001924000000154 Published online by Cambridge University Press

7. JACKSON, W. (Ed) Wake vortex prediction: an overview, Appendix F: hazard definition, 2001, Transportation Department of Canada TP 13629E.
8. ABRAMOWITZ, M. and STEGUN, I. *Tables of Mathematical Functions*, 1965, Dover, New York.
9. HINTON, D.A. and TATNALL, C.R. A candidate wake vortex strength definition for application to the NASA aircraft vortex space system (AVOSS), 1997, NASA Tech. Memo TM-110343.
10. LAMB, H. *Hydrodynamics*, 1932, Sixth edition, Cambridge University Press.
11. HOFFMAN, E.R. and JOUBERT, P.N. Turbulent line vortices, *J Fluid Mech*, 1963, **16**, pp 395-411.
12. HALLOCK, J.N. and BURNHAM, D.C. Decay characteristics of wake vortex from jet transport aircraft, 1997, AIAA paper 97-0060, 35th Aerospace Science Meeting Exhibition, 9-10 Jan 1997, Reno, NV.
13. PROCTOR, F.H. The NASA-Langley wake vortex modeling effort in support of an operational aircraft spacing system, 1998, AIAA paper 98-0589.
14. LIGHTHILL, M.J. *An Informal Introduction to Fluid Mechanics*, 1986 Oxford University Press.
15. MILNE-THOMSON, L.M. *Theoretical Aerodynamics*, 1958, Dover, New York.
16. ABOTT, I.H. and DOENHOFF, A.E. *Theory of Wing Sections*, 1959, Dover, New York.
17. TATNALL, C.R. A Proposed Methodology for Determining Wake-Vortex Imposed Aircraft Separation Constraints, 1995, MSc thesis submitted at George Washington University.
18. BATCHELOR, G.K. *Fluid Mechanics*, 1967, Cambridge University Press.
19. CARSLAW, H.S. and JAEGER, J.C. *Heat Conduction in Solids*, 1949, Oxford University Press.
20. LANDAU, L.D. and LIFSHITZ, E.F. *Fluid Mechanics*, 1953, Pergamon, Oxford.
21. JACKSON, P. (Ed) *Jane's All-the-World's Aircraft 2000-2001*, 2000, MacDonald and Jane's, London.
22. STUERVER, R.A. Airplane data base for wake-vortex hazard definition and assessment, 1995, Version 2.0, NASA Langley Research Center.
23. HOZÄPFEL, F. A probabilistic two-phase wake vortex decay and transport model, 2000, DLR Institut für Physik der Atmosphäre rep 163, Oberpfaffenhofen.
24. CAMPBELL, S.D., DASEY, T.J., FREEHART, R.E., HEINRICHS, R.M., MATTHEWS, M.P., PERRAS, G.H. and ROWE, G.S. Wake Vortex Filed Measurement Program at Memphis, TN, Data Guide, 1997, Lincoln Lab, Massachusetts Inst of Technology, Project Rep NASA/L-2, Cambridge, MA.

https://doi.org/10.1017/S0001924000000154 Published online by Cambridge University Press